Angular distributions and total cross sections for D^- formation from interaction of D^+ and D^0 with cesium*

Carmen Cisneros and Ignacio Alvarez
Instituto de Fisica, México, 20, D.F.
C. F. Barnett and J. A. Ray
Oak Ridge National Laboratory, Oak Ridge, Tennessee 37830
(Received 1 December 1975; revised manuscript received 22 March 1976)

Absolute differential scattering cross sections have been determined for single and double electron-capture collisions of 0.5- to 2.5-keV D^+ and D^0 in Cs vapor. Integration of the differential cross section over the scattering angles yielded the total electron-capture cross sections. Angular distributions were peaked in the forward direction, and the angular width increased as the particle energy decreased. Cross sections for both single and double capture processes decreased with increasing energy.

I. INTRODUCTION

Formation of high-intensity negative-ion beams has long been of interest in tandem electrostatic accelerators. Within the past few years the interest has been expanded to other fields where needs have developed in meson factories, high-energy ion implantation, surface studies, simulation of neutron damage in reactor materials, and heating of fusion reactor plasmas. A method proposed to heat a magnetically confined toroidal plasma above temperatures obtainable with Ohmic heating is to inject 150–1000-keV D atoms. These atoms are trapped in the magnetic field by ionization and transfer energy to the low-energy Maxwellian plasma through Coulomb collisions, thereby heating the plasma. Cross sections for D^0 formation in this energy range are small for either electron-capture or dissociative collisions. To overcome this difficulty the suggestion has been made to accelerate D^- ions to 150–1000 keV and pass the negative ions through a gas stripping cell whose conversion efficiency for D^0 is 70–80%. Two methods presently exist for production of D^- beams: (1) direct extraction from an ion source, and (2) passage of 1–5-keV D^+, D_2^+, or D_3^+ ions through an alkaline vapor cell which has a high conversion efficiency for D^- production. The cross sections for D^- production by electron capture collisions have been measured by several investigators.[1-4] The D^- ions formed in this manner would be accelerated to the higher energies before reaching the stripping cell. Until only recently[5] the yield of D^- from sources has been very modest. Thus it seems that the most attractive route to obtain D^- was through electron-capture collisions in Cs vapor with deuterium ion beams that are presently available.

If D^- is to be efficiently accelerated, the angular distribution of D^- emerging from a vapor cell must be known, such that cell geometry and beam optics will be optimized. In this paper we report the absolute differential scattering cross sections for D^- formation in Cs vapor in the energy region 0.5–2.5 keV. These differential scattering cross sections are integrated over the scattering angles to obtain the total single and double elecron-capture cross sections. Obtaining the total cross section by integration of the differential cross section differs from the method of other investigators,[1-4] who have measured the total cross section directly for D^- production under single-collision conditions.

Angular scattering measurements are described for multiple collisions under near-charge-equilibrium conditions. Measurements of D^- equilibrium fractions are discussed along with the difficulties encountered in obtaining the data. Single and multiple scattering has been characterized by determining the cone angle into which 50%[$\theta(0.5)$] and 90%[$\theta(0.9)$] of the D^- are scattered.

II. APPARATUS AND MEASUREMENTS

A. General description

The apparatus shown in Fig. 1 is essentially the same as that used for the study of angular distributions of H^+ and D^+ in the electron stripping of H^0 and D^0 atoms in N_2.[6,7] The apparatus consists basically of four parts: ion source, neutralization cell, scattering chamber, and detector chambers.

A deuterium ion beam was extracted from a duoplasmatron ion source, accelerated to 0.5–2.5 keV, magnetically mass analyzed, and collimated. The desired ions entered the argon neutralization cell, where electron-capture collisions converted a fraction of the beam to D^0. The beam on emerging from the gas cell was passed through a set of transverse electrostatic deflection plates which deflected the charged component of the beam and also quenched the metastable D(2s) state. The

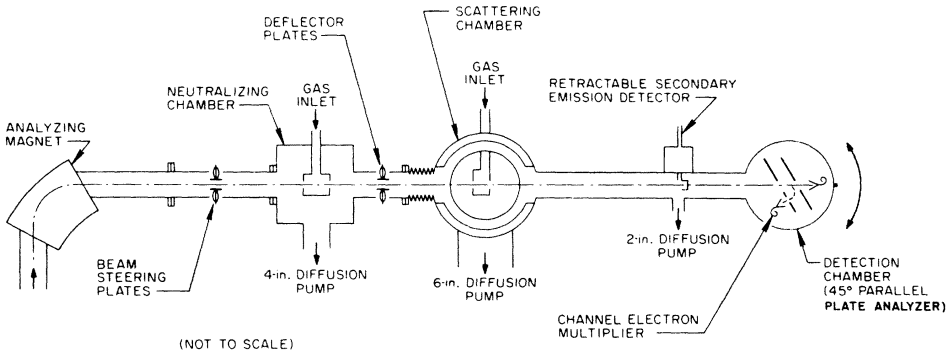

FIG. 1. Schematic diagram of apparatus.

argon cell was evacuated for D^+ cross-section measurements. Either ions or atoms entered the Cs interaction cell, where D^- ions were formed.

The entire detector assembly rotated about the axis of the Cs-vapor cell. Provisions were made for rotations up to $\pm 45°$, although the exit aperture of the Cs cell limited useful scans to $\pm 7°$. Between the Cs cell and detector assembly, a retractable Faraday cup for secondary emission measured the total beam. The detector chamber housed a parabolic 45° electrostatic analyzer with two funnel-type channel electron multipliers.

B. Cesium cell

The cesium cell was made of a stainless-steel block 3.9 cm wide and 2.8 cm long. Mounted by a screw connection to the collision chamber was the cesium reservoir, 2.5 cm long and 1.5 cm in diameter. The 1-mm-diam entrance aperture was milled to a knife edge to minimize slit scattering, whereas the exit aperture was a 2×6 mm slit. The scattering chamber was heated by four tantalum wire coils wound on a quartz rod and placed in four cavities bored lengthwise in the stainless-steel block. With the screw-type connection the temperature in the collision chamber was always greater by a few degrees than that of the Cs reservoir, such that the Cs-vapor density could be determined from the reservoir temperature.

Chromel-Alumel thermocouples were attached to the Cs cell and the reservoir. The thermocouples were calibrated at 100 and 0 °C, with the temperature being known to an accuracy of better than 0.5 °C. Data were taken for reservoir temperatures from 75 to 160 °C. The Cs-vapor density was calculated from available vapor-pressure data.[8-10] Cesium-vapor density-temperature data were taken from thse papers, and a curve was fitted to the data points, as shown in Fig. 2; we used these values in relating temperature to Cs-vapor density.

Attached to the sides of the collision chamber were two water-cooled copper plates which quickly reduced the cell temperature when water flowed through the cooling system. To prevent Cs vapor from contaminating the vacuum system and detectors, the Cs cell and oven were placed inside a water-cooled cylinder 12 cm in diameter. This entire assembly was pumped with a liquid-nitrogen-trapped diffusion pump. For Cs-vapor pressures of 10^{-3} Torr the pressure in the region surrounding the cell was less than 5×10^{-7} Torr.

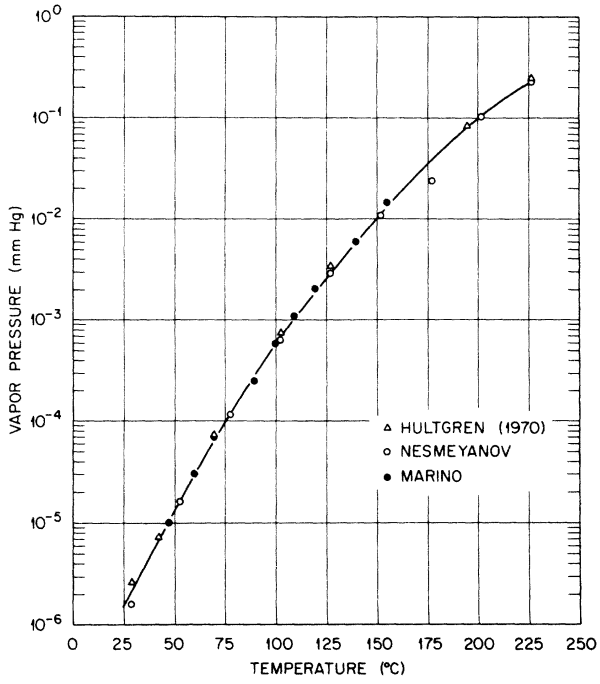

FIG. 2. Vapor pressure of Cs as a function of the oven temperature. The data have been derived from an evaluated set of Cs-vapor pressures of Hultgren, published values by Nesmeianov and measurements by Marino *et al.*

C. Detection system

The detection system is the same as that described previously[6] and included a Faraday-cup secondary-emission detector. The D^+ was measured directly, and the D^0 flux was measured first by determining the secondary emission coefficient for D^+ on the copper target and then assuming that the emission coefficient was the same for D^+ and D^0 in this energy range.[11] During the measurements with Cs in the collision cell and with incident D^0, the total D^0 beam was assumed to be the sum of D^+ and D^0, as measured by secondary emission. The secondary-emission coefficient was measured frequently; when changes greater than 10% were observed, the detector was cleaned.

The 45° parabolic analyzer has been described by Harrower.[12] An aperture was cut in the rear plate of the analyzer such that the neutral beam entering through the entrance aperture (1 mm) could be monitored. Both the ion and neutral components were counted by funnel-type channel electron multipliers. Since the total beam was measured by a secondary-emission detector, careful precautions were taken in converting the D^--multiplier counting rate to current flow. To make this conversion the D^- and D^+ counting efficiency was calibrated by comparing a known D^- or D^+ beam, as measured by a Faraday cup, with the multiplier counting rate. Since channel electron multipliers saturate at low counting rates, it was necessary to calibrate the multiplier at counting rates less than 10^5 sec^{-1} and operate in the charge-saturated mode.

Shown in Fig. 3 are the counting efficiencies as a function of energy for both D^- and D^+ when the front end of the multiplier was grounded and the collector end was maintained at -3 kV. In addition, the front of the multiplier was covered with a 94% transmission grid to ensure uniform response over the multiplier aperture. The data shown were corrected for this transmission factor.

In this experiment the basic angular distribution is smeared owing to three factors: the angular distribution of the beam entering the cesium cell (θ_B), the finite resolution of the ion detection (θ_D), and the finite size of the reacting volume (θ_V), which can contribute to the smearing owing to the beam radial dimensions and the vapor cell length. From the geometric configuration the resolutions were calculated as follows: $\theta_B = 0.5$ mrad; $\theta_D = 1.9$ mrad; $\theta_V \leq 1.8$ mrad (for angles less than 1°). The total resolution can be characterized by the root-mean-square resolution of 2.7 mrad (0.15°). The expected resolution corresponds closely to the measured resolution of the neutral beam.

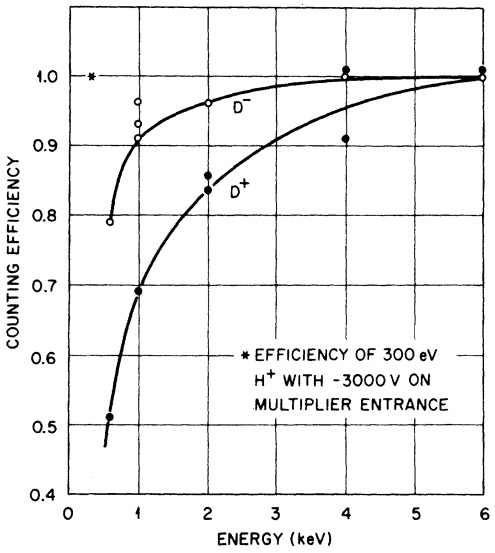

FIG. 3. Efficiency of a funnel-type channel electron multiplier for D^- and D^+ ions. Multiplier entrance grounded.

D. Procedure

With D^+ or D^0 incident on the Cs cell, the total current I_0 was measured by the secondary-emission detector. The D^- $[I(\theta, \phi)]$ scattered through a solid angle $d\Omega$ was determined by the channel multiplier as the assembly was rotated about the Cs-cell axis. Both sides of the 0° scattering angle were scanned to ensure symmetry and to locate the 0° angle. The differential scattering cross section was determined by the relation $d\sigma = I(\theta, \phi)\, d\Omega / I_0 n l$, where n is the target density corrected to standard temperature (273 °C) and l is the effective path length. The total cross section was derived by integrating the differential cross section over θ and ϕ:

$$\sigma_{i-} = 2\pi \int_0^{\theta} \frac{d\sigma_{i-}}{d\Omega} \sin\theta \, d\theta ,$$

where i is the incident charge state, 0 or +. Equilibrium values were determined by increasing the Cs-vapor density to the values where $I^-(\theta, \phi)/I_0$ was independent of n. Integrating these values of $I^-(\theta, \phi)$ and dividing by I_0 resulted in the equilibrium fraction of D^-.

E. Errors

Several sources of errors are present. Possible sources of systematic errors are as follows: (1) effective path length, (2) density determination,

(3) measurements of total beam, (4) angular resolution and integration, (5) energy spread of the scattered beam, and (6) detector calibration. The geometric path length of the Cs cell was 2.54 cm. Because of molecular streaming of the Cs, the geometric path length must be increased. This length has been increased by the sum of the entrance aperture diameter and the effective exit diameter, which was defined as the diameter of a circle whose area is equal to that of the 2×6 mm slit. The effective path length was 3.03 cm when these corrections were added to the geometric length. This is a 19% correction. The error to the path length from this correction was estimated to be no more than ±4%.

The largest source of error in the present measurements arose from the determination of the Cs density. To assess this error is very difficult; probably the best assessment is the scatter of the data points in Fig. 2. At 105 °C the scatter in the vapor-density data is ±23%. The uncertainty in the temperature added another ±2% to this error, giving a total uncertainty of ±25%.

In determining the incident D^0 intensity, the assumption was made that the secondary-emission coefficients of D^+ and D^0 were equal at the same energy. Previous measurements[11] have shown that the secondary-emission coefficient for H^0 was greater than that of H^+ for energies greater than 20 keV. Extrapolation of this data to the present energy indicated that we underestimated the D^0 flux by 5%. This error did not apply to the D^+ flux determination.

In integrating the differential cross section to obtain the total cross section, the first step was to multiply $d\sigma$ by $\sin\theta$ before integrating over θ. In essence this gave the scattering into an angular ring $d\theta$. As θ approaches zero, the quantity $I^-(\theta) \times \sin\theta$ approaches zero, as shown in Fig. 4 for five D^+ energies. This behavior is a result of the finite solid angle of the detector and angular resolution of the finite solid angle of the detector and angular resolution of the beam geometry. However, in a following paper we have shown that if one integrates the $I(\theta)\sin\theta$ vs θ curve, total cross sections were obtainable that were within a few percent of the total cross sections measured directly. No corrections to the data have been made for this feature.

Cross sections would be underestimated if the energy acceptance window of the multiplier was less than the energy spread of the D^- beam. The energy resolution of the analyzer was 11%. At 5 keV the energy window was 55 eV wide, which was greater than the energy spread of the D^- scattered beam. This was verified by scanning the D^- beam across the analyzer exit aperture

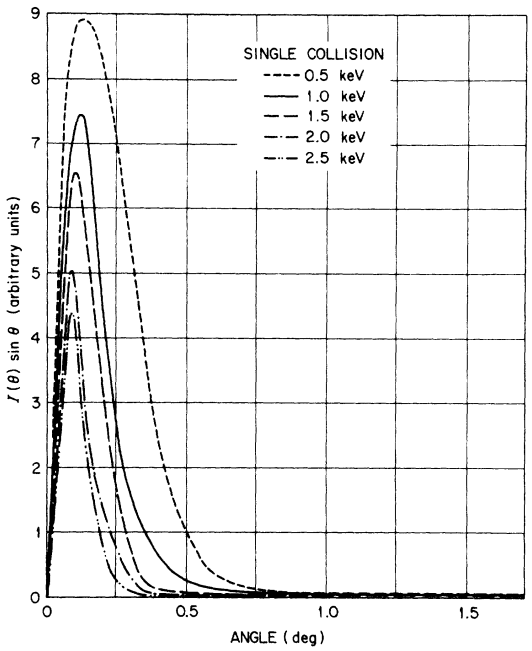

FIG. 4. $I(\theta)\sin\theta$ as a function of scattering angle for 0.5–2.5-keV D^+ in a Cs cell forming D^- under single-collision conditions.

(1 cm) and determining the beam profile. The profile was flat in the central region, indicating that the total D^- beam was being measured by the detector. The detector calibration was probably within ±3%. The total error involved in the cross-section data is best expressed as the root-mean-square error of ±26%.

An additional difficulty was encountered in measuring the particle currents at high cesium target densities ($nl \rightarrow 6 \times 10^{14}$ cm^{-2}). At target densities approaching equilibrium charge conditions, the D^--fraction data points scattered by ±30%.

III. RESULTS AND DISCUSSION

In measuring the double electron-capture cross sections, precautions must be taken to assure that the measurements were made under single-collision conditions. Usually the procedure involves detecting the formation of the negative ion as the collision-cell pressure is increased, which should result in a linear slope for the negative fraction as a function of the pressure. For double electron capture of protons in hydrogen, the linear section of the curve is valid only over a small region above the residual pressure. In the present measurements a more sensitive indication of single-collision conditions exists. The shape of the differential scattering cross sections should be independent of the cesium target density.

Shown in Fig. 5 are the differential scattering cross sections for double electron capture for 1-keV deuterons in cesium at target densities (nl) between 2.8×10^{13} and 2.2×10^{14} cm^{-2}. For the lowest densities both the magnitude and shape of the cross sections are the same within the experimental error. All cross sections were taken with target densities less than 3×10^{13} cm^{-2}. Similar results were obtained for 1.5-keV D^0 in cesium vapor; the differential cross sections are shown in Fig. 6 for the single-capture process. In this case the cross sections were less sensitive to target density than for the double electron-capture process. As can be seen in both Figs. 5 and 6, the scattering from the electron-capture processes is predominately in the forward direction, which is characteristic of small momentum transfer in electron-capture collisions. In all cases, as the target density is increased to the pressure at which multiple collisions prevail, the angular distributions become wider. For example, as the target density was increased from 2.8×10^{13} to 9.6×10^{14} cm^{-2}, the angle at which the differential cross section was 9×10^{-15} cm^2 increased from 0.6° to 2.2°.

The differential scattering cross sections for the double electron capture ($D^+ + Cs \rightarrow D^- + Cs^{2+}$) are shown in Fig. 7 for energies of 0.5–3.0 keV. It is interesting to observe that the cross sections for 0° scattering fluctuates only 10% from a mean value for the five different energies, whereas at 2° scattering the cross section decreased by a factor of 2.5 as the energy was increased from 0.5 to 2.5 keV. Similar data for the single electron-capture process ($D^0 + Cs \rightarrow D^- + Cs^+$) are shown in Fig. 8.

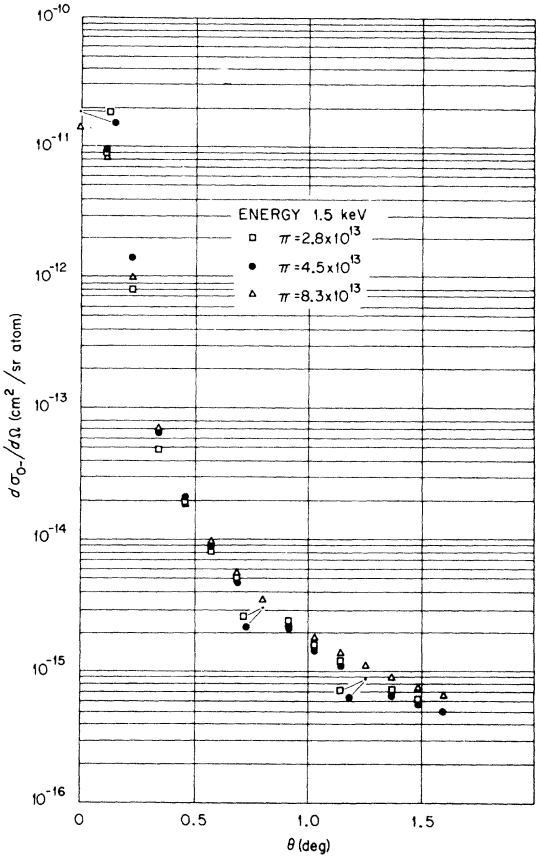

FIG. 6. Differential scattering cross sections for D^- formation by 1.5-keV D^0 incident on Cs vapor as a function of the scattering angle for three Cs target densities.

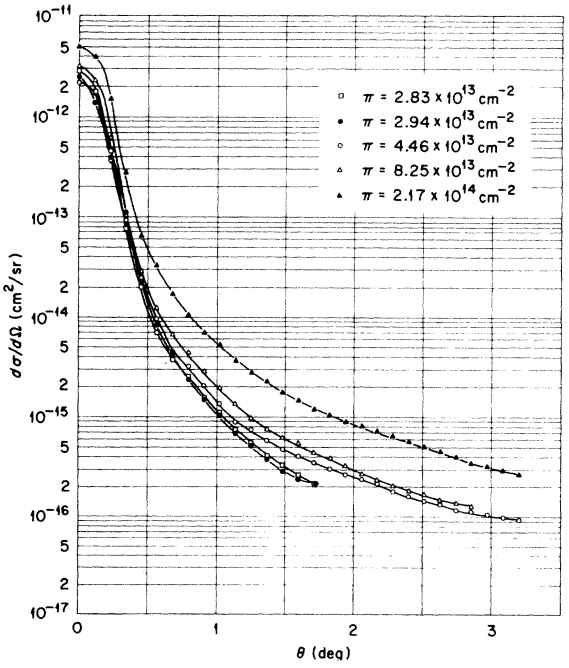

FIG. 5. Differential scattering cross sections for D^- formation by 1-keV D^+ incident on Cs vapor as a function of the scattering angle for five Cs target densities.

Integration of the differential cross sections to obtain the total cross sections involves first plotting the quantity $I(\theta)\sin\theta\, d\theta$ as a function of θ and obtaining plots similar to those shown in Fig. 4. The value of $I(\theta)\sin\theta\, d\theta$ is the scattering cross section into an annular cone of width $d\theta$. These curves are integrated over θ to obtain the total cross sections, as shown in Fig. 9 for both the double and single electron-capture processes. The data indicate that the single electron-capture cross section σ_{0-} is a maximum at energies of 0.5–1.0 keV. As the incident energy decreases, the double electron-capture cross section increases down to the lowest energy at which the cross section is measured. This energy dependence was unexpected, since the second Cs

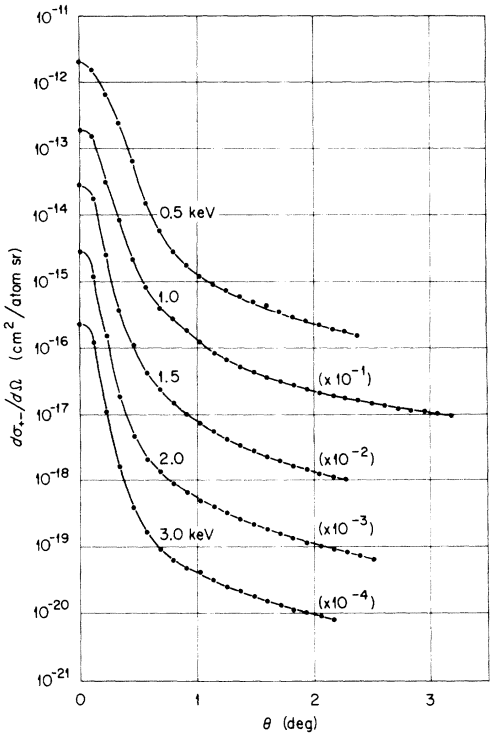

FIG. 7. Differential scattering cross sections for the inelastic collision $D^+ + Cs \rightarrow D^- + Cs^{2+}$.

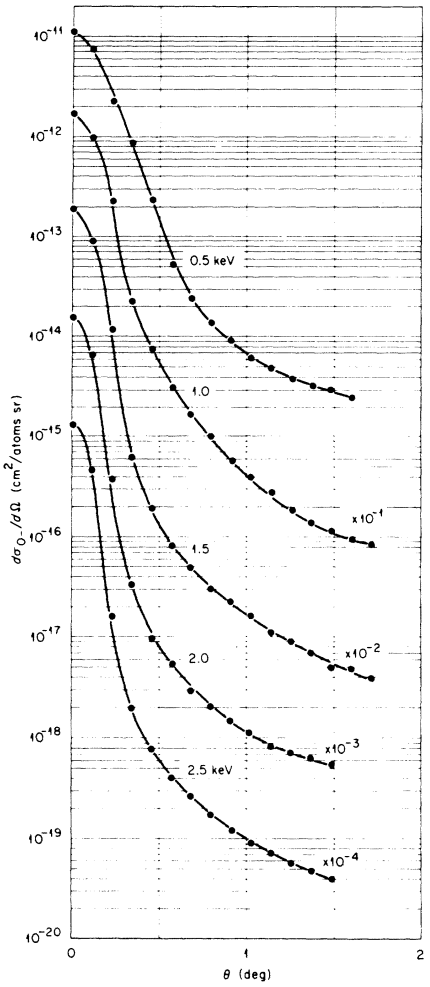

FIG. 8. Differential scattering cross sections for the inelastic collisions $D^0 + Cs \rightarrow D^- + Cs^+$.

electron is bound by 25.1 eV. This behavior suggests that the single collision is a two-step process involving curve crossing. At some distance R_1, as the deuteron approaches the Cs atom, the separated atom potential curve crosses the $2s$ or $2p$ level of the $D(n=2)Cs^+$ curve. For some collisions the D atom penetrates further until a crossing of the D^-Cs^{2+} curve forms a D^- ion and leaves a Cs^{2+} ion. Thus it is possible through curve crossing to have a two-step process in a single collision. This process is examined in more detail for double electron capture of D_2^+ to form D^- in one of the following papers.

Also shown in Fig. 9 are the results for single electron-capture cross sections as measured by Schlachter *et al.*[2] for D^0 in Cs. At 2 keV their results are 50% greater than the present results, and the cross sections decrease more slowly with increasing energy than in the present measurements. The double electron-capture cross sections are compared with Grüebler *et al.*[3] in Fig. 9. Again the cross sections of Grüebler *et al.* are higher, but the energy dependence is approximately the same as in the present results. Both measurements of σ_{1-1} are within the experimental error.

D^- equilibrium fractions were determined as a function of D^+ and D^0 incident energy. The fraction decreased from 0.10 at 0.5 keV to 0.04 at 2.5 keV. These values are less (as much as a factor of 2–3) than the equilibrium fractions measured by Schlachter *et al.*[2] and Meyer and Anderson[4] for incident deuterium particles and by Bohlen *et al.*[1] and Grüebler *et al.*[3] for equivelocity protons. The energy dependence of the present measurements and those of Grüebler *et al.* and Meyer and Anderson are essentially the same. No evidence was found of a maximum in the negative fraction at 1.5 keV, as found by Schlachter.

D^- fractions for incident D^0 were consistently less than those for incident D^+ by approximately 10%, which implies a Cs-vapor density less than that required for charge equilibrium. Measurements by Pradel *et al.*[13] indicated the minimum cesium target thickness for charge equilibration, using a 1-keV D^+ beam, was at least 1.2×10^{15}

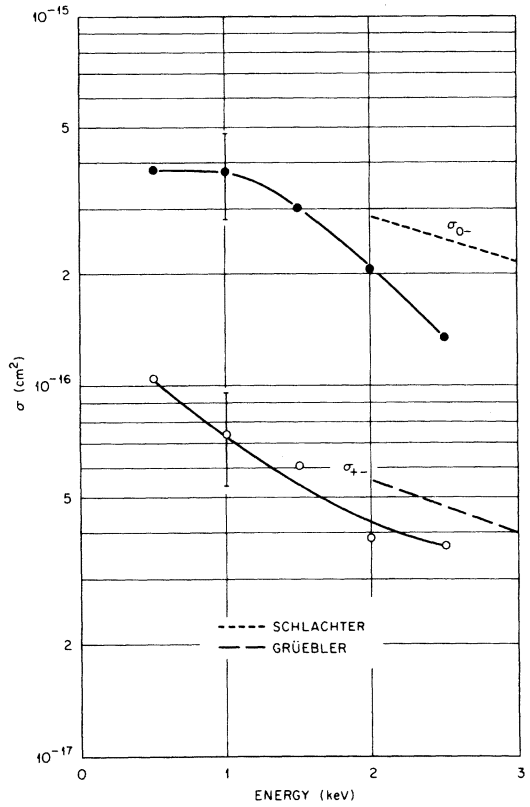

FIG. 9. Total cross sections for double electron capture (σ_{1-1}) and single electron capture (σ_{0-1}) for deuterium particles in Cs vapor. Plotted for comparison are the D^0 measurements of Schlachter *et al.*[2] for σ_{0-1} and H^+ measurements of Grüebler *et al.*[3] for σ_{1-1}. The H^+ energies have been multiplied by 2 for comparison.

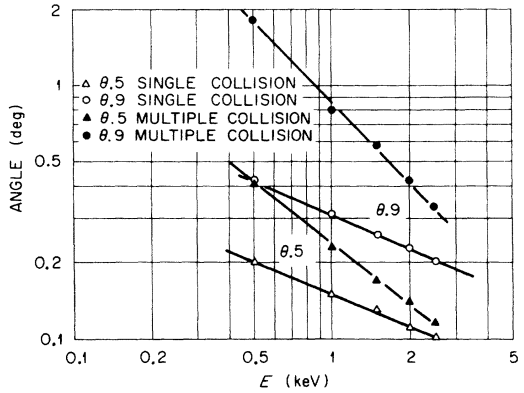

FIG. 10. Cone angles into which 50% and 90% of the D^- are scattered for single and multiple collisions. D^+ incident on Cs. $nl \sim 8\times10^{14}$ cm^{-2} for multiple-collisions measurement.

cm^{-2}. Because of the cesium-cell geometry, the maximum cesium target density was 9×10^{14} cm^{-2}. This lower density would result in an underestimation of the D^- fraction by 17%. However, a plot of the D^- differential cross sections integrated over all scattering angles as a function of the Cs-vapor density indicated saturation of the D^- fraction within the scatter (± 30%) of the data points at the higher vapor densities. Other equilibrium measurements with D_2^+ incident on the cesium cell indicated that charge equilibrium was not achieved at the highest cesium density obtainable. With incident D_3^+ the D^- fraction per incident nucleon was the same as that D^+ or D^0 at comparable target densities [$(7-9)\times10^{14}$ cm^{-2}]. These observations suggest that the D_3^+ ion captures an electron with a high degree of probability into the repulsive ground state of the D_3 molecule, which immediately forms three D^0, whereas D_2^+ captures an electron into the stable ground state. At these energies, the probability or cross section of D_2 collisional ioinization or direct D_2^+ dissociation is small compared to the electron-capture cross section. Thus the target thickness would be greater for producing charge equilibrium for D_2^+ than for D^+ or D_3^+.

Of great importance to the designer of a negative-ion accelerator in which the negative ions are produced in a vapor cell is the angular divergence of the negative-ion beam as it leaves the vapor cell. We have chosen to characterize the angular divergence as the cone angle into which 50% [$\theta(0.5)$] and 90% [$\theta(0.9)$] of the negative beam is scattered. The cone angles for D^- formation as a function of the D^+ incident energy are shown in Fig. 10, and for the D^0 incident energy in Fig. 11

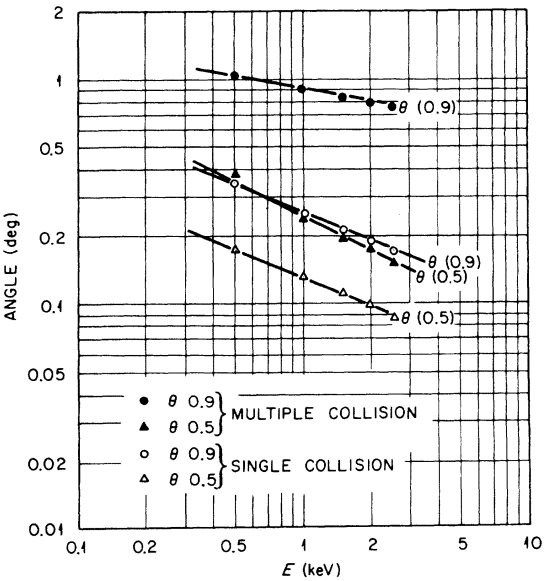

FIG. 11. Cone angles into which 50% and 90% of the D^- are scattered for single and multiple collisions. D^0 incident on Cs. $nl \sim 8\times10^{14}$ cm^{-2} for multiple-collisions measurement.

for both single and multiple collisions. For both D^+ and D^0 incident the D^- ions were contained in a cone less than 0.4° at 0.5 keV and less than 0.1° at 2.5 keV under single-collision conditions. For single collisons the cone angles into which 50% of D^- is contained were essentially the same for either D^+ or D^- incident. For multiple collisions ($nl \sim 8 \times 10^{14}$ cm^{-2}) the $\theta(0.5)$ curves are the same, within experimental error, for D^+ and D^0 incident on the cesium cell. However, both the magnitude of the scattering angle and energy dependence are different for $\theta(0.9)$ with D^+ and D^0 incident. These results were repeatable within the experimental accuracy of the measurements. One would expect that under equilibrium target densities the $\theta(0.9)$ curve would be independent of the charge of the incident particle.

The discrepancy in the magnitude of the D^- equilibrium fraction by a factor of 2–3 is surprising, since this is a rather easy parameter to measure. In the present measurements the target gas density needed to produce charge equilibruim may be low, such that the quoted equilibrium fractions are low by 20%. However, the largest uncertainty probably arises from the difficulty in determining the absolute D^0 current in the presence of Cs vapor. We are unable to elucidate the D^- scattering into $\theta(0.9)$ cone angles at the present time. Further experimentation is planned to explore the interactions of D^+, D^0, D_2^+, and D_3^+ at the higher Cs-vapor pressures.

ACKNOWLEDGMENT

We appreciate the stimulating discussions and many helpful comments of Professor A. Russek of the University of Connecticut.

---

*Work supported by the U. S. Energy Research and Development Administration under a contract with Union Carbide Corporation.

[1]H. Bohlen, G. Clausnitzer, and H. Wilsen, Z. Phys. 208, 159 (1968).

[2]A. S. Schlachter, P. J. Borkholm, D. H. Loyd, L. W. Anderson, and W. Haeberli, Phys. Rev. 177, 184 (1969).

[3]W. Grüebler, P. A. Schnelgback, V. Koning, and P. Marmier, Helv. Phys. Acta 43, 254 (1970).

[4]F. W. Meyer and L. W. Anderson, Phys. Rev. A 11, 589 (1975).

[5]Yu. I. Bel'chenko, G. I. Dimov, and V. G. Dudnikov, Zh. Tekh. Fiz. 45, 68 (1975) [Sov. Phys.-Tech. Phys. 20, 40 (1975)].

[6]H. H. Fleischmann, C. F. Barnett, and J. A. Ray, Phys. Rev. A 10, 569 (1974).

[7]C. Cisneros, I. Alverez, C. F. Barnett, and J. A. Ray, following paper [Phys. Rev. A 14, 84 (1976)].

[8]A. N. Nesmeianov, *Vapor Pressures of the Elements*, translated and edited by J. I. Carasso (Academic, New York, 1961).

[9]L. L. Marino, A.C. H. Smit, and E. Caplinger, Phys. Rev. 128, 2243 (1962).

[10]R. H. Hultgren, R. L. Orr, P. D. Anderson, and K. K. Kelley, *Selected Values of Thermodynamic Properties of Metals and Alloys* (Wiley, New York, 1963), p. 85. Present data taken from supplement issued in 1970.

[11]P. M. Stier, C. F. Barnett, and G. E. Evans, Phys. Rev. 96, 973 (1954).

[12]G. A. Harrower, Rev. Sci. Instrum. 26, 850 (1955).

[13]P. Pradel, F. Roussel, A. S. Schlachter, G. Spiess, and A. Valance, Phys. Rev. A 10, 797 (1974).